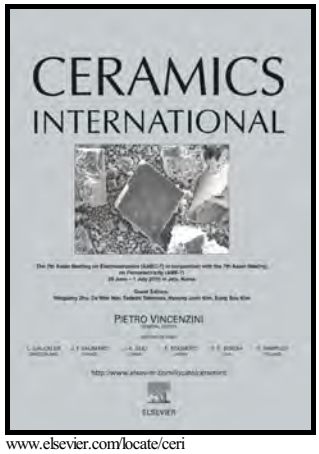

www.elsevier.com/locate/ceri

Correlations between the Structural Characteristics and Enhanced Microwave Dielectric Properties of V–Modified $Li_3Mg_2NbO_6$ Ceramics

Gang Wang, Huaiwu Zhang, Xin Huang, Fang Xu, Gongwen Gan, Yan Yang, Dandan Wen, Jie Li, Cheng Liu, Lichuan Jin

PII: S0272-8842(18)31886-8
DOI: https://doi.org/10.1016/j.ceramint.2018.07.156
Reference: CERI18878

To appear in: *Ceramics International*

Received date: 6 June 2018
Revised date: 13 July 2018
Accepted date: 17 July 2018

Cite this article as: Gang Wang, Huaiwu Zhang, Xin Huang, Fang Xu, Gongwen Gan, Yan Yang, Dandan Wen, Jie Li, Cheng Liu and Lichuan Jin, Correlations between the Structural Characteristics and Enhanced Microwave Dielectric Properties of V–Modified $Li_3Mg_2NbO_6$ Ceramics, *Ceramics International,* https://doi.org/10.1016/j.ceramint.2018.07.156

Correlations between the Structural Characteristics and Enhanced Microwave Dielectric Properties of V–Modified $Li_3Mg_2NbO_6$ Ceramics

Gang Wang*, Huaiwu Zhang*, Xin Huang, Fang Xu, Gongwen Gan, Yan Yang, Dandan Wen, Jie Li, Cheng Liu, Lichuan Jin

State Key Laboratory of Electronic Thin Films and Integrated Devices, University of Electronic Science and Technology of China, Chengdu 610054, China

Abstract

Novel low-temperature fired $Li_3Mg_2Nb_{1-x}V_xO_6$ (x=0.02–0.08) microwave dielectric ceramics were synthetized by the partial substitution of V^{5+} ions on the Nb^{5+} sites. The effects of V^{5+} substitution on structure and microwave dielectric properties were investigated in detail. XRD patterns and Rietveld refinement demonstrated that all of the samples exhibited a single orthorhombic structure. The structural characteristics such as the polarizability, packing fraction and NbO_6 octahedron distortion were determined to establish the correlations between the structure and the microwave dielectric characteristics. The ε_r values presented a tendency similar to that of the polarizability. The high $Q\times f$ values were mainly attributed to the effects of the grain sizes and density rather than the packing fraction. The variation in the τ_f values was attributed to NbO_6 octahedron distortion. Notably, the $Li_3Mg_2Nb_{1-x}V_xO_6$ (x=0.02) ceramics sintered at 900 °C had outstanding microwave dielectric properties: ε_r=16, $Q\times f$=131,000 GHz (9.63 GHz), and τ_f=−26 ppm/°C, making these ceramics promising ultralow loss candidates for low temperature co-fired ceramics (LTCC) applications.

Keywords: $Li_3Mg_2Nb_{1-x}V_xO_6$ ceramics, structural characteristics, correlations

* Corresponding author:
Email address: wang_toward@163.com; hwzhang@uestc.edu.cn

Introduction

In the past decades, microwave dielectric materials have attracted increasing attention for their superior performance in passive components such as capacitors, filters, and resonators [1-3]. Low temperature co-fired ceramics (LTCC) technology has received much attention due to the demand for system miniaturization and integration [4]. Dielectric materials with a low sintering temperature (<960 °C) and excellent chemical compatibility with Ag electrodes are essential for LTCC applications [5]. However, most microwave dielectric ceramics must be sintered at a high temperature. Therefore, it is important to reduce the sintering temperature of dielectric materials to satisfy the requirements of LTCC applications. To lower the sintering temperature of ceramics, several approaches have used the addition of glass frits and low-melting oxides [6-8]. Due to the degraded microwave dielectric characteristics caused by glass frits, it is essential to develop new LTCC systems with excellent performances characteristics [9-13].

Recently, $Li_3Mg_2NbO_6$ ceramics with an orthorhombic structure have attracted increased attention due to their good performance. M. Castellanos et al. prepared the $Li_3Mg_2NbO_6$ phase by heating the mixtures of Li_3NbO_4 and MgO and holding at 1270 K for 4 d [14]. Bian et al. reported that $Li_3Mg_2NbO_6$ ceramics have good microwave dielectric properties, namely, ε_r=16.8, $Q\times f$=79643 GHz, and τ_f=−27.2 ppm/°C[15]. Since then, many research studies have been conducted to achieve low temperature sintering and improve the $Q\times f$ values. Zuo et al. reported low-temperature sintered $Li_3(Mg_{0.92}Zn_{0.08})_2NbO_6$ ceramics doped with Li_2O-V_2O_5[16]. Zhang et al. also reported that the $Li_3Mg_2NbO_6$ ceramics possess excellent dielectric properties, namely, ε_r=14.89, $Q\times f$=86720 GHz, and τ_f=−15.46 ppm/°C when doped with 1wt. % Li_2O-B_2O_3-SiO_2

glass. However, all of the materials described above are sintered at a low temperature with liquid-phase addition, possibly deteriorating the microwave dielectric properties. Therefore, many studies have been performed to lower the sintering temperature through ions substitution [17-19]. For instance, Wang et al. successfully lowered the sintering temperature of $ZnNb_2O_6$ ceramics by V^{5+} substitution[20]. Zuo et al. found that V^{5+} could diffuse into $Li_3(Mg_{0.92}Zn_{0.08})_2NbO_6$ and lower the sintering temperature[21]. Furthermore, the cation radii of V^{5+} (0.54 Å) and Nb^{5+} (0.64 Å) are similar and solid solutions are predicted to form in $Li_3Mg_2NbO_6$ systems for V^{5+} substitution.

In this work, $Li_3Mg_2Nb_{1-x}V_xO_6$ solid solutions were synthesized through the solid-state reaction route. The effects of V^{5+} substitution on the morphology, structural characteristics and microwave dielectric properties were studied systematically. Based on the Rietveld refinement results, intrinsic characteristics including the polarizability, packing fraction and NbO_6 octahedron distortion were determined. Finally, the relationships between the structural characteristics and the enhanced microwave dielectric properties were established.

Experiment procedure

$Li_3Mg_2Nb_{1-x}V_xO_6$ (x=0.02, 0.04, 0.06, 0.08) ceramics were synthesized through the solid-state reaction route using the Li_2CO_3, MgO, Nb_2O_5 and V_2O_5 precursors (all with purity>99%). The raw materials were weighed and ball-milled in distilled water for 4 h in a nylon jar. The obtained slurry was dried and calcined at 800 °C for 4 h. Then, the calcined powders were ball-milled again for another 4 h, and then the mixture was mixed with polyvinyl alcohol (PVA) and pressed into cylindrical disks (12 mm in diameter and 6 mm in thickness). The pellets were sintered at 850 °C – 1000 °C for 4 h.

The bulk densities were measured by the Archimedes method using distilled water as buoyancy media. The crystalline phase was analyzed using X-ray diffractometer (XRD: Model Miniflex 600, Rigaku Co., Japan) with CuKα radiation and 2θ angle scans were conducted from 10° to 120°, with a step width of 0.02°. The structure refinements were performed by Rietveld's method using the GSAS suit of programs with the EXPGUI software [22]. The microstructures and grain sizes were observed using a scanning electron microscope (JSM-6490, Japan). The microwave dielectric properties were measured by the Hakki-Coleman dielectric resonator method with a network analyzer (Agilent N5230A, USA). The value of the temperature coefficient of the resonant frequency value (TCF, τ_f) can be calculated by the following equation:

$$\tau_f = \frac{f_{80} - f_{20}}{f_{20} \times 60} \times 10^6 \text{ (ppm/°C)}, \quad (1)$$

where f_{80} and f_{20} are the resonant frequencies at 80 °C and 20°C, respectively.

Results and discussion

The XRD patterns of the $Li_3Mg_2Nb_{1-x}V_xO_6$ ceramics sintered at 900 °C are shown in Fig. 1. All of the samples exhibited the single-phase orthorhombic structure of $Li_3Mg_2NbO_6$ (JCPDS#86-0346) and no significant second phase could be observed within the detection limit of the instrument. This observation indicated that continuous solid solutions were formed throughout the entire substitution range. Additionally, the diffraction peak of the (206) crystal plane shifted toward higher diffraction angles with the increase in the value of x, indicating that the unit cell volume decreased gradually. This could be attributed to the decrease of the ionic radius on the Nb^{5+} site due to the smaller ionic radius of V^{5+} ions (0.54 Å), compared to that of the Nb^{5+} ions (0.64 Å).

To obtain detailed information for the lattice parameters, unit cell volume and bond lengths, Rietveld refinements were conducted on the $Li_3Mg_2Nb_{1-x}V_xO_6$ samples using the GSAS suite of programs with the EXPGUI software. The orthorhombic $Li_3Mg_2NbO_6$ structure was adopted as the initial model. For the crystal structure model of $Li_3Mg_2NbO_6$ phase, each primitive cell contained eight $Li_3Mg_2NbO_6$ formula units. All of the divalent and univalent cations occupied the (A-) site and pentavalent cations occupied the (B-) site, with the A-site ions occupying the 8b and 16g Wyckoff positions and the B-site ions occupying the 8a Wyckoff position[23]. Fig. 2 shows the representative plots of the experimental (red circle) and calculated (blue line) XRD data for the $Li_3Mg_2Nb_{1-x}V_xO_6$ ceramics with (a) x = 0.02 and (b) x= 0.04. It was obvious that

the calculated curves agreed with the measured patterns and the positions of the Bragg reflections were nearly consistent with the indexed peaks. These results proved that the single-phase orthorhombic $Li_3Mg_2NbO_6$ structure ceramics were obtained. The constants, unit cell volumes and the reliability factors (R_p, R_{wp} and χ^2) of the $Li_3Mg_2Nb_{1-x}V_xO_6$ ceramics are summarized in Table 1. With the increase of the V^{5+} substituent content, the lattice parameters and the unit cell volume decreased, which was consistent with the diffraction peak of the (206) crystal plane shifting toward high diffraction angles, as shown in Fig. 1(b). The fitting parameters R_p (reliability factor of the weighted patterns) and R_{wp} (reliability factor of the patterns) were smaller than 15%, and χ^2 (goodness of fit indicator) ranged from 2 to 3, indicating that the obtained refinement results were highly reliable. The bond lengths and the distortion of the NbO_6 octahedron were utilized to explore the correlation between the structural characteristics and the temperature coefficient of the resonant frequency, as presented in Table 2.

Fig. 3 shows the SEM micrographs of the $Li_3Mg_2Nb_{1-x}V_xO_6$ ceramics sintered at 900 °C. It is clear that the grain sizes and pores were greatly affected by the composition. As shown in Fig. 3, clear grain boundaries could be observed for all of the samples, indicating that all of the samples could be sintered well at 900 °C and no visible liquid phase appeared. For $x \leq 0.04$, dense and homogeneous microstructures were obtained, which indicated that a moderate amount of V^{5+} substitution could significantly improve the densification of the $Li_3Mg_2Nb_{1-x}V_xO_6$ ceramics, as shown in

Figs. 3(a)-(b). Especially, the samples with x=0.02 exhibited a more dense and uniform microstructure with larger grain size, signifying a lower dielectric loss. However, excessive V^{5+} substitution promoted abnormal grain growth and nonuniform microstructures with pores and some relatively smaller grains were observed as shown in Figs. 3(c)-(d), which demonstrated that the densities of the $Li_3Mg_2Nb_{1-x}V_xO_6$ ceramics decreased. Especially, the highly doped $Li_3Mg_2Nb_{1-x}V_xO_6$ composition (x=0.08) exhibited a nonuniform microstructure with an inhomogeneous grain distribution, thus deteriorating the microwave dielectric performances characteristics. The average grain size(D) can be calculated using the linear intercept method [24]:

$$D = \frac{3L}{2MN}, \tag{2}$$

where M, L and N are the actual magnification, the length of test line and the number of intercepts, respectively. As the V^{5+} content increased, the calculated average grain sizes were 14.1,10.4, 9.3, and 7.5μm, respectively. These results indicated that a moderate amount of V^{5+} substitution (0.02 mol V^{5+} substitution for Nb^{5+} ions) could promote the grain growth.

To determine the effects of the V^{5+} substitution on the bulk densities and sintering temperature of the $Li_3Mg_2Nb_{1-x}V_xO_6$ ceramics, the apparent densities of the $Li_3Mg_2Nb_{1-x}V_xO_6$ ceramics sintered at different temperatures are shown in Fig. 4. The bulk density of pure $Li_3Mg_2NbO_6$ was adopted as the reference with its value ranging from 3.5 g/cm^3 to 3.6 g/cm^3 [25, 26]. Since the sintering temperature ranged from

850 °C to 1000 °C, the apparent densities of the $Li_3Mg_2Nb_{1-x}V_xO_6$ ceramics increased reaching a maximum (higher than the density of the pure $Li_3Mg_2NbO_6$ ceramics) at approximately 900 °C and then decreasing. The results indicated that V^{5+} substitution on the Nb^{5+} sites could reduce the sintering temperature to 900 °C and densify the $Li_3Mg_2Nb_{1-x}V_xO_6$ ceramics. Previous studies have revealed that the substitution of Nb^{5+} ions by V^{5+} ions in $ZnNb_2O_6$ ceramics also lowered the sintering temperature [20]. Specifically, the apparent densities of the $Li_3Mg_2Nb_{1-x}V_xO_6$ ceramics decreased with the increase of the V^{5+} content when sintered at 900 °C, suggesting that an appropriate V^{5+} substitution (x=0.02) was sufficient to densify the $Li_3Mg_2Nb_{1-x}V_xO_6$ ceramics at 900 °C, in agreement with the SEM micrographs, as illustrated in Fig. 3.

Fig. 5 presents the dielectric constant of the $Li_3Mg_2Nb_{1-x}V_xO_6$ ceramics sintered at 850°C – 1000°C. Generally, the dielectric constant is related to many factors, such as the bulk density, second phase, ionic polarizability, and structural characteristics[27, 28]. As shown in Fig. 1, no obvious second phase could be observed within the detection limit of the instrument, which indicated that the dielectric constant variation was mainly attributed to the changes in the density and ionic polarizability. The relationships between the dielectric constant and the apparent densities as well as dielectric polarizabilities could be explained using the Clausius-Mosotti equation [29]:

$$\frac{\varepsilon_r - 1}{\varepsilon_r + 2} = \frac{N\alpha}{3\varepsilon_0}, \tag{3}$$

where ε_r and ε_0 are the dielectric constants of the dielectric ceramics and vacuum,

respectively. α is the molecules polarizability (total polarizability). N is the number of molecules per unit volume, which is equivalent to the density. As presented in Fig. 5, with the increasing temperature, the dielectric constant of the $Li_3Mg_2Nb_{1-x}V_xO_6$ ceramics first increased reaching a maximum approximately 900 °C and then decreased, which was consistent with the variation of the apparent densities. For the samples sintered at the optimized temperature (900 °C), the dielectric constant decreased with the increase of the V^{5+} substitution content, which is related to the decrease of the densities and the smaller ionic polarizability of V^{5+} (2.92 $Å^3$), compared to that of Nb^{5+} (3.97 $Å^3$). To determine the influences of the densification and polarizability on the dielectric constant of $Li_3Mg_2Nb_{1-x}V_xO_6$ ceramics, the dielectric constant could be revised by the following equation[30]:

$$\varepsilon_{mea} = \varepsilon_{rc}\left(1 - \frac{3p(\varepsilon_{rc} - 1)}{2\varepsilon_{rc} + 1}\right), \tag{4}$$

where ε_{mea} and ε_{rc} are the measured dielectric constant and the porosity corrected dielectric constant, respectively. p is the porosity fraction. The theoretical densities of the $Li_3Mg_2Nb_{1-x}V_xO_6$ ceramics obtained from the Rietveld refinement were 3.82, 3.81, 3.8, and 3.8 g/cm^3, respectively. The observed dielectric polarizabilities (α_{obs}) could be calculated by Eq.(5) using the porosity corrected dielectric constan[31, 32], while the theoretical dielectric polarizabilities (α_{theo}) were obtained by Eq.(6)[33].

$$\alpha_{obs} = \frac{V_m}{b}\frac{(\varepsilon_{rc} - 1)}{(\varepsilon_{rc} + 2)} \tag{5}$$

$$\alpha_{theo} = 3\alpha\left(Li^{+}\right) + 2\alpha\left(Mg^{2+}\right) + (1-x)\alpha\left(Nb^{5+}\right) + x\alpha\left(V^{5+}\right) + 6\alpha\left(O^{2-}\right), \quad (6)$$

Where α (Li^{+}) =1.20 Å^3, α (Mg^{2+}) =1.32 Å^3, α (Nb^{5+}) =3.97 Å^3, α (V^{5+}) =2.92 Å^3 and α (O^{2-}) =2.01 Å^3 are oxide polarizabilities[31]. V_m and b are the molar volume and a constant ($4\pi/3$), respectively. The ε_{mea}, ε_{rc}, α_{obs} and α_{theo} values are presented in Table 3. The porosity-corrected dielectric constant (ε_{rc}) decreased with the increase of the V^{5+} substituent content, which was similar to the variation of the measured dielectric constant (ε_{mea}). Moreover, the theoretical dielectric polarizabilities (α_{theo}) and observed dielectric polarizabilities (α_{obs}) also decreased with the decreased with increasing x, and only an extremely small discrepancy between the values of α_{theo} and α_{obs} with the deviation of $\Delta = |(\alpha_{theo}-\alpha_{obs})/\ \alpha_{obs}\times 100\%| \leq 1\%$ was found, indicating that the observed dielectric polarizabilities (α_{obs}) matched well with the theoretical dielectric polarizabilities (α_{theo}). Furthermore, the α_{obs} was slightly higher than α_{theo}, which might be attributed to "structural changes" such as polyhedral distortion [34, 35].

The $Q\times f$ values of $Li_3Mg_2Nb_{1-x}V_xO_6$ ceramics are demonstrated in Fig. 6. It has been reported that the dielectric losses are affected by many factors categorized as the intrinsic factors and the extrinsic factors. The intrinsic factors include structural characteristics such as the atomic packing fraction, while the extrinsic factors consisted of the second phase, the grain sizes, and densification [35, 36]. As shown in Fig. 1, all of the samples exhibited a single orthorhombic structure, indicating that the effects of the second phase could be eliminated. Therefore, the $Q\times f$ values were affected by the

packing fraction, grain size, and density. As the sintering temperature increased, the $Q\times f$ values first increased, reaching a maximum and then decreased. For the samples sintered at the optimized temperature (900 °C), the $Q\times f$ values decreased with the increase in the V^{5+} content. The above results indicated that the diversification of the $Q\times f$ values exhibited a similar tendency as the variation in the density, implying that the apparent density influenced the $Q\times f$ values. Additionally, the grain boundaries gave rise to an extrinsic loss by acting as two-dimensional defects, while the increase of the grain sizes decreased the total content of the grain boundaries [37]. Therefore, the grain sizes contributed to the $Q\times f$ values. To explore the relationships between the $Q\times f$ values and the intrinsic factor, the packing fraction (P.F) was obtained as follows [38]:

$$\text{Packing fraction}=\frac{\text{volume of the atoms in the cell}}{\text{volume of unit cell}}\times Z, \quad (7)$$

where Z=8 for the $Li_3Mg_2Nb_{1-x}V_xO_6$ ceramics. The obtained density, grain sizes and packing fraction are summarized in Table 4. For the $Li_3Mg_2Nb_{1-x}V_xO_6$ ceramics sintered at 900 °C, the $Q\times f$ values decreased with increased V^{5+} content, which was in agreement with the variation in the density and the grain sizes. Particularly, the $Q\times f$ values presented a trend that was opposite to that for the packing fraction. Therefore, the $Q\times f$ values were mainly controlled by the integrated effects originated from the density, the grain sizes and the packing fraction, whereas the extrinsic factors (the density and the grain sizes) dominated. Remarkably, the $Li_3Mg_2Nb_{1-x}V_xO_6$ (x=0.02) ceramics sintered at 900 °C possessed extraordinarily high $Q\times f$ =131,000 GHz. There are several

reasons for the very high $Q\times f$ values of the $Li_3Mg_2Nb_{1-x}V_xO_6$ (x=0.02) ceramics sintered at 900 °C. First, $Li_3Mg_2Nb_{1-x}V_xO_6$ (x=0.02) ceramics exhibited a single orthorhombic $Li_3Mg_2NbO_6$ structure phase (JCPDS#86-0346), compared to the study by Zuo et al [16]. Second , the $Li_3Mg_2Nb_{1-x}V_xO_6$ (x=0.02) ceramics sintered at 900 °C cured lithium volatilization unlike for the results reported by Wu et al [26]. Third, the high density and large grain size contributed to the high $Q\times f$ values of the $Li_3Mg_2Nb_{1-x}V_xO_6$ (x=0.02) ceramics.

It is well-known that the temperature coefficient of the resonant frequency (τ_f) depends on the temperature coefficient of the dielectric constant (τ_ε) as described by:

$$\tau_f = -\alpha - \frac{1}{2}\tau_\varepsilon, \tag{8}$$

where α is the linear thermal expansion coefficient (~10 ppm/°C) while τ_ε is related to the structural characteristics, such as the octahedral distortions. The distortion (δ) could be calculated according to the bond length of NbO_6 octahedron, as given by [39]:

$$\delta = \frac{1}{6}\sum\left(\frac{R_i - \overline{R}}{\overline{R}}\right)^2, \tag{9}$$

where R_i is the individual bond length, and $\overline{R}$ represents the average bond length of the NbO_6 octahedron. The correlation between the τ_f values and the NbO_6 octahedron distortion for the $Li_3Mg_2Nb_{1-x}V_xO_6$ ceramics sintered at 900 °C is revealed in Fig. 7. The τ_f values increased from -26 ppm/°C to -6 ppm/°C with the substitution of the V^{5+} for the Nb^{5+} ions, which was in accordance with the variations of the NbO_6 octahedron distortion. This observation indicated that the τ_f values were affected by the NbO_6

octahedron distortion.

Conclusions

$Li_3Mg_2Nb_{1-x}V_xO_6$ (x=0.02-0.08) ceramics were synthesized through the solid-state reaction route. The effects of V5+ substitution on the structure and microwave dielectric characteristics were investigated systematically. XRD patterns and Rietveld refinement proved that all of the samples exhibited a single orthorhombic structure throughout the entire substitution range. The lattice parameters and unit cell volume decreased with the increase of the V^{5+} content, as was confirmed by the slightly higher 2θ angles of the (206) peak. The structural parameters such as the packing fraction, polarizability and NbO_6 octahedron distortion were calculated based on the Rietveld refinement. The ε_r values showed a tendency similar to the tendency of the polarizability and the observed dielectric polarizability was nearly identical to the theoretical dielectric polarizability. The high $Q\times f$ values were mainly attributed to the effects of the density and grain sizes rather than the packing fraction. The variation in the τ_f values was related to the variations of the NbO_6 octahedron distortion. Remarkably, the $Li_3Mg_2Nb_{1-x}V_xO_6$ (x=0.02) ceramics sintered at 900 °C possessed outstanding properties, namely, ε_r=16, $Q\times f$ =131,000 GHz, and τ_f=−26 ppm/°C, making them promising candidates for ultra-low loss LTCC applications.

Acknowledgements

This work was financially supported by the National Key Research and Development Plan (No. 2016YFA0300801 and 2017YFB0406300), the National Natural Science Foundation of China (Grant Nos. 51402041, 51602036 and 51672036), the Scientific Research Launch Foundation of UESTC (Grant No. ZYGX2016KYQD092), the National High-Tech Research and Development Program of China (Grant No. 2015AA034102), the Sichuan Key research projects (Nos. 2017GZ0408 and 2017GZ0415), the Guizhou Province Key R&D Program (2016-3011), and the Science and Technology Department of Sichuan Province (Grant No. 2014GZ0015).

References

[1] S.J. Fiedziuszko, I.C. Hunter, T. Itoh, Y. Kobayashi, T. Nishikawa, S.N. Stitzer, K. Wakino, Dielectric materials, devices, and circuits, IEEE Trans. Microw. Theory Tech. 50 (2002) 706-720.

[2] W. Wersing, Microwave ceramics for resonators and filters, Curr. Opin. Solid St. M. 1 (1996) 715-731.

[3] I.M. Reaney, D. Iddles, Microwave dielectric ceramics for resonators and filters in mobile phone networks, J. Am. Ceram. Soc. 89 (2006) 2063-2072.

[4] M.T. Sebastian, H. Jantunen, Low loss dielectric materials for LTCC applications: a review, Int. Mater. Rev. 53 (2008) 57-90.

[5] M.T. Sebastian, Dielectric Materials for Wireless Communication, Elsevier Oxford, 2008.

[6] S. Zhang, H. Su, H. Zhang, Y. Jing, X. Tang, Microwave dielectric properties of $CaWO_4$–Li_2TiO_3 ceramics added with LBSCA glass for LTCC applications, Ceram. Int. 42 (2016) 15242-15246.

[7] H. Shao, Z. Liu, G. Jian, Y. Li, Low-temperature sintering of $Ti_{1-x}Cu_{x/3}Nb_{2x/3}O_2$ (x = 0.23) microwave dielectric ceramics with CuO and B_2O_3 addition, Ceram. Int. 44 (2018) 3314-3318.

[8] Q. Guo, L. Li, S. Yu, Z. Sun, H. Zheng, J. Li, W. Luo, Temperature–stable dielectrics based on Cu–doped $Bi_2Mg_{2/3}Nb_{4/3}O_7$ pyrochlore ceramics for LTCC, Ceram. Int. 44 (2018) 333-338.

[9] S.Z. Hao, D. Zhou, W.B. Li, L.X. Pang, Microwave Dielectric Properties of $BiCu_2PO_6$ Ceramics with Low Sintering Temperature, J. Electron. Mater. 46 (2017) 6241-6245.

[10] W.J. Luo, L.X. Li, Q.Y. Guo, X.S. Lv, Crystal structure and dielectric properties of Mn-substituted $Bi_{1.5}Zn_{1.0}Nb_{1.5}O_7$ pyrochlore ceramics as temperature stable LTCC material, J. Mater. Sci.-Mater. Electron. 28 (2017) 5623-5627.

[11] D. Zhou, C.A. Randall, L.-X. Pang, H. Wang, J. Guo, G.-Q. Zhang, X.-G. Wu, L. Shui, X. Yao, Microwave Dielectric Properties of Li_2WO_4 Ceramic with Ultra-Low Sintering Temperature, J. Am. Ceram. Soc. 94 (2011) 348-350.

[12] Q. Liao, L. Li, X. Ren, X. Yu, D. Guo, M. Wang, A Low Sintering Temperature Low Loss Microwave Dielectric Material $ZnZrNb_2O_8$, J. Am. Ceram. Soc. 95 (2012) 3363-3365.

[13] D. Zhou, J. Guo, X. Yao, L.X. Pang, Z.M. Qi, T. Shao, Phase evolution and microwave dielectric properties of $(Li_{0.5}Bi_{0.5})(W_{1-x}Mo_x)O_4$ ($0.0 \leq x \leq 1.0$) ceramics with ultra-low sintering temperatures, Funct. Mater. Lett. 5 (2012) 1250042

[14] M. Castellanos, J.A. Gard, A.R. West, Crystal data for a new family of phases, $Li_3Mg_2XO_6$:X=Nb, Ta, Sb, J. Appl. Crystallogr. 15 (1982) 116-119.

[15] L.L. Yuan, J.J. Bian, Microwave Dielectric Properties of the Lithium Containing Compounds with Rock Salt Structure, Ferroelectrics 387 (2009) 123-129.

[16] T. Zhang, R. Zuo, Effect of Li_2O-V_2O_5 addition on the sintering behavior and microwave dielectric properties of $Li_3(Mg_{1-x}Zn_x)_2NbO_6$ ceramics, Ceram. Int. 40 (2014) 15677-15684.

[17] D. Zhou, H. Wang, X. Yao, Y. Liu, Microwave dielectric properties of low-firing $BiNbO_4$ ceramics with V_2O_5 substitution, J. Electroceram. 21 (2008) 469-472.

[18] D. Zhou, L.-X. Pang, X. Yao, H. Wang, Influence of sintering process on the microwave dielectric properties of $Bi(V_{0.008}Nb_{0.992})O_4$ ceramics, Mater. Chem. Phys. 115 (2009) 126-131.

[19] L.X. Pang, D. Zhou, D.W. Wang, J.X. Zhao, W.G. Liu, Z.X. Yue, I. M. Reaney, Temperature stable $K_{0.5}(Nd_{1-x}Bi_x)_{0.5}MoO_4$ microwave dielectrics ceramics with ultra -

low sintering temperature, J. Am. Ceram. Soc. 101 (2018) 1806-1810.

[20] J. Wang, Z.X. Yue, Z.L. Gui, L.T. Li, Low-temperature sintered $Zn(Nb_{1-x}V_{x/2})_2O_{6-2.5x}$ microwave dielectric ceramics with high Q value for LTCC application, J. Alloy. Compd. 392 (2005) 263-267.

[21] T. Zhang, R. Zuo, C. Zhang, Preparation and microwave dielectric properties of $Li_3(Mg_{0.92}Zn_{0.08})_2NbO_6$-$Ba_3(VO_4)_2$ composite ceramics for LTCC applications, Mater. Res. Bull. 68 (2015) 109-114.

[22] B.H. Toby, EXPGUI, a graphical user interface for GSAS, J. Appl. Crystallogr. 34 (2001) 210-213.

[23] G.C. Mather, R.I. Smith, J.M.S. Skakle, J.G. Fletcher, M.A. Castellanos R, M.P. Gutierrez, A.R. West, Synthesis and structures of the partially ordered rock salt phases, $Li_3M_2XO_6$: M=Mg, Co, Ni; X=Nb, Ta, Sb, J. Mater. Chem. 5 (1995) 1177-1182.

[24] H. Zheng, S. Yu, L. Li, X. Lyu, Z. Sun, S. Chen, Crystal structure, mixture behavior, and microwave dielectric properties of novel temperature stable $(1-x)MgMoO_4-xTiO_2$ composite ceramics, J. Eur. Ceram. Soc. 37 (2017) 4661-4665.

[25] H.T. Wu, E.S. Kim, Characterization of low loss microwave dielectric materials $Li_3Mg_2NbO_6$ based on the chemical bond theory, J. Alloy. Compd. 669 (2016) 134-140.

[26] C.F. Xing, J.X. Bi, H.T. Wu, Effect of Co-substitution on microwave dielectric properties of $Li_3(Mg_{1-x}Co_x)_2NbO_6$ ($0.00 \leq x \leq 0.10$) ceramics, J. Alloy. Compd. 719 (2017) 58-62.

[27] P. Zhang, H. Xie, Y. Zhao, X. Zhao, M. Xiao, Low temperature sintering and microwave dielectric properties of $Li_3Mg_2NbO_6$ ceramics doped with $Li_2O–B_2O_3–SiO_2$ glass, J. Alloy. Compd. 690 (2017) 688-691.

[28] P. Zhang, Y.G. Zhao, L.X. Li, The correlations among bond ionicity, lattice energy and microwave dielectric properties of $(Nd_{1-x}La_x)NbO_4$ ceramics, Phys. Chem. Chem. Phys. 17 (2015) 16692-16698.

[29] K. Maex, M.R. Baklanov, D. Shamiryan, F. lacopi, S.H. Brongersma, Z.S. Yanovitskaya, Low dielectric constant materials for microelectronics, J. Appl. Phys. 93 (2003) 8793-8841.

[30] S.J. Penn, N.M. Alford, A. Templeton, X.R. Wang, M.S. Xu, M. Reece, K. Schrapel, Effect of porosity and grain size on the microwave dielectric properties of sintered alumina, J. Am. Ceram. Soc. 80 (1997) 1885-1888.

[31] R.D. Shannon, Dielectric Polarizabilities of Ions in Oxides and Fluorides, J. Appl. Phys. 73 (1993) 348-366.

[32] C.L. Huang, W.R. Yang, P.C. Yu, High-Q microwave dielectrics in low-temperature sintered $(Zn_{1-x}Ni_x)_3Nb_2O_8$ ceramics, J. Eur. Ceram. Soc. 34 (2014) 277-284.

[33] R.D. Shannon, G.R. Rossman, Dielectric constants of silicate garnets and the oxide additivity rule, Am. Mineral. 77 (1992) 94-100.

[34] H. Wu, E.S. Kim, Correlations between crystal structure and dielectric properties of high-Q materials in rock-salt structure Li_2O-MgO-BO_2 (B = Ti, Sn, Zr) systems at

microwave frequency, RSC Advances 6 (2016) 47443-47453.

[35] Z. Fu, P. Liu, J. Ma, X. Zhao, H. Zhang, Novel series of ultra-low loss microwave dielectric ceramics: $Li_2Mg_3BO_6$ (B=Ti, Sn, Zr), J. Eur. Ceram. Soc. 36 (2016) 625-629.

[36] E.S. Kim, B.S. Chun, R. Freer, R.J. Cernik, Effects of packing fraction and bond valence on microwave dielectric properties of $A^{2+}B^{6+}O_4$ (A2+: Ca, Pb, Ba; B6+: Mo, W) ceramics, J. Eur. Ceram. Soc. 30 (2010) 1731-1736.

[37] N. Ichinose, T. Shimada, Effect of grain size and secondary phase on microwave dielectric properties of $Ba(Mg_{1/3}Ta_{2/3})O_3$ and $Ba([Mg,Zn]_{1/3}Ta_{2/3})O_3$ systems, J. Eur. Ceram. Soc. 26 (2006) 1755-1759.

[38] H.L. Pan, L. Cheng, H.T. Wu, Relationships between crystal structure and microwave dielectric properties of $Li_2(Mg_{1-x}Co_x)_3TiO_6$ ($0 \leq x \leq 0.4$) ceramics, Ceram. Int. 43 (2017) 15018-15026.

[39] Y. Li, X. Lu, Y. Zhang, Y. Zou, L. Wang, H. Zhu, Z. Fu, Q. Zhang, Characterization of $Co_{0.5}(Ti_{1-x}Zr_x)_{0.5}NbO_4$ microwave dielectric ceramics based on structural refinement, Ceram. Int. 43 (2017) 11516-11522.

Figure Captions:

Fig. 1. XRD patterns of the $Li_3Mg_2Nb_{1-x}V_xO_6$ ceramics sintered at 900 °C (a) and variation of the (206) diffraction peak (b).

Fig. 2. Rietveld refinements of the $Li_3Mg_2Nb_{1-x}V_xO_6$ ceramics sintered at 900 °C for 4 h, (a) x = 0.02 and (b) x= 0.04.

Fig. 3. SEM micrographs of the $Li_3Mg_2Nb_{1-x}V_xO_6$ ceramics sintered at 900 °C. (a)x=0.02,(b)x=0.04,(c)x=0.06,(d)x=0.08.

Fig. 4. Apparent densities of the $Li_3Mg_2Nb_{1-x}V_xO_6$ (x=0.02–0.08) ceramics sintered at 850 °C–950 °C for 4 h.

Fig. 5. Dielectric constant of the $Li_3Mg_2Nb_{1-x}V_xO_6$ (x=0.02–0.08) ceramics sintered at 850 °C–950 °C for 4 h.

Fig. 6. $Q\times f$ values of the $Li_3Mg_2Nb_{1-x}V_xO_6$ (x=0.02–0.08) ceramics sintered at 850 °C–950 °C for 4 h.

Fig. 7.τ_f values and the NbO_6 octahedron distortions for the $Li_3Mg_2Nb_{1-x}V_xO_6$ ceramics sintered at 900 °C.

Tab. 1

The lattice parameters, unit cell volume and the reliability factors of $Li_3Mg_2Nb_{1-x}V_xO_6$ (x=0.02–0.04) ceramics sintered at 900 °C

x	0.02	0.04	0.06	0.08

a(Å)	5.90144	5.90115	5.90076	5.89697
b(Å)	8.54477	8.54176	8.54033	8.53499
c(Å)	17.74024	17.73889	17.73716	17.7262
V($Å^3$)	894.577	894.15	893.853	892.17
P.F. (%)	70.3767	70.4025	70.418064	70.543
R_p(%)χ^2	5.88	6.14	7.88	7.3
R_{wp}(%)	7.47	7.82	10	9.44
χ^2	2.1	2.4	2.6	2.8

Tab. 2

The bond lengths and the distortion of the NbO_6 octahedron of $Li_3Mg_2Nb_{1-x}V_xO_6$ (x=0.02–0.04) ceramics sintered at 900 °C

Type	x=0.02	x=0.04	x=0.06	x=0.08
Nb-O(1)×2	1.9808	1.9801	1.97965	1.97842
Nb-O(2)×4	1.9992	1.9987	1.99855	1.99829
$\overline{R}$	1.9931	1.9925	1.99225	1.99167
δ	0.0017%	0.0019%	0.0020%	0.00221

Tab. 3

The the measured dielectric constant (ε_{mea}), porosity corrected dielectric constant (ε_{rc}) , observed dielectric polarizabilities (α_{obs}) and theoretical dielectric polarizabilities (α_{theo})values of $Li_3Mg_2Nb_{1-x}V_xO_6$ (x=0.02–0.04) ceramics sintered at 900 °C

x	0.02	0.04	0.06	0.08
p	2.6%	4%	4.8%	5%
ε_{mea}	16.01	15.62	15.40	15.18
ε_{rc}	16.6	16.52	16.48	16.29
α_{obs}	22.39	22.36	22.34	22.26
α_{theo}	22.25	22.23	22.2	22.18
Δ	0.63%	0.58%	0.63%	0.36%

Tab. 4

The density, grain sizes and packing fraction of $Li_3Mg_2Nb_{1-x}V_xO_6$ (x=0.02–0.04) ceramics sintered at 900 °C.

x	0.02	0.04	0.06	0.08
density	97.4%	96%	95.2%	95%
grain sizes	14.1	10.4	9.3	7.5
P.F(%)	70.38	70.40	70.42	70.54
$Q\times f$ (10^4GHz)	13.1	10.7	9.0	7.2

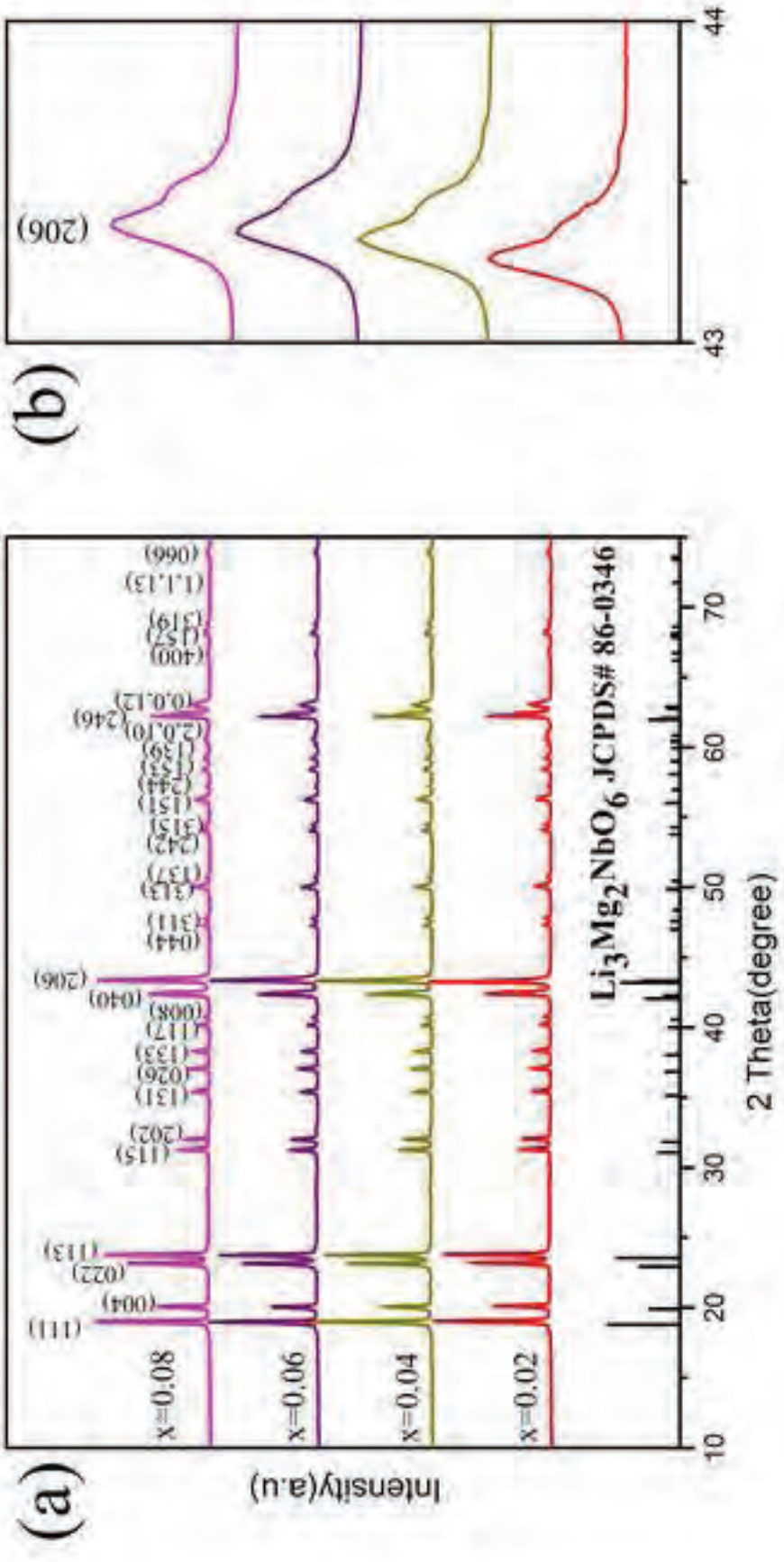
(a)
Intensity(a.u)
x=0.08
x=0.06
x=0.04
x=0.02
(111)
(004)
(022)
(113)
(115)
(202)
(131)
(026)
(133)
(117)
(008)
(040)
(206)
(044)
(311)
(313)
(137)
(242)
(315)
(151)
(244)
(153)
(139)
(2,0,10)
(246)
(0,0,12)
(400)
(157)
(319)
(1,1,13)
(066)
Li3Mg2NbO6 JCPDS# 86-0346
2 Theta(degree)
10
20
30
40
50
60
70
(b)
(206)
43
44

Figure 1

Figure 2

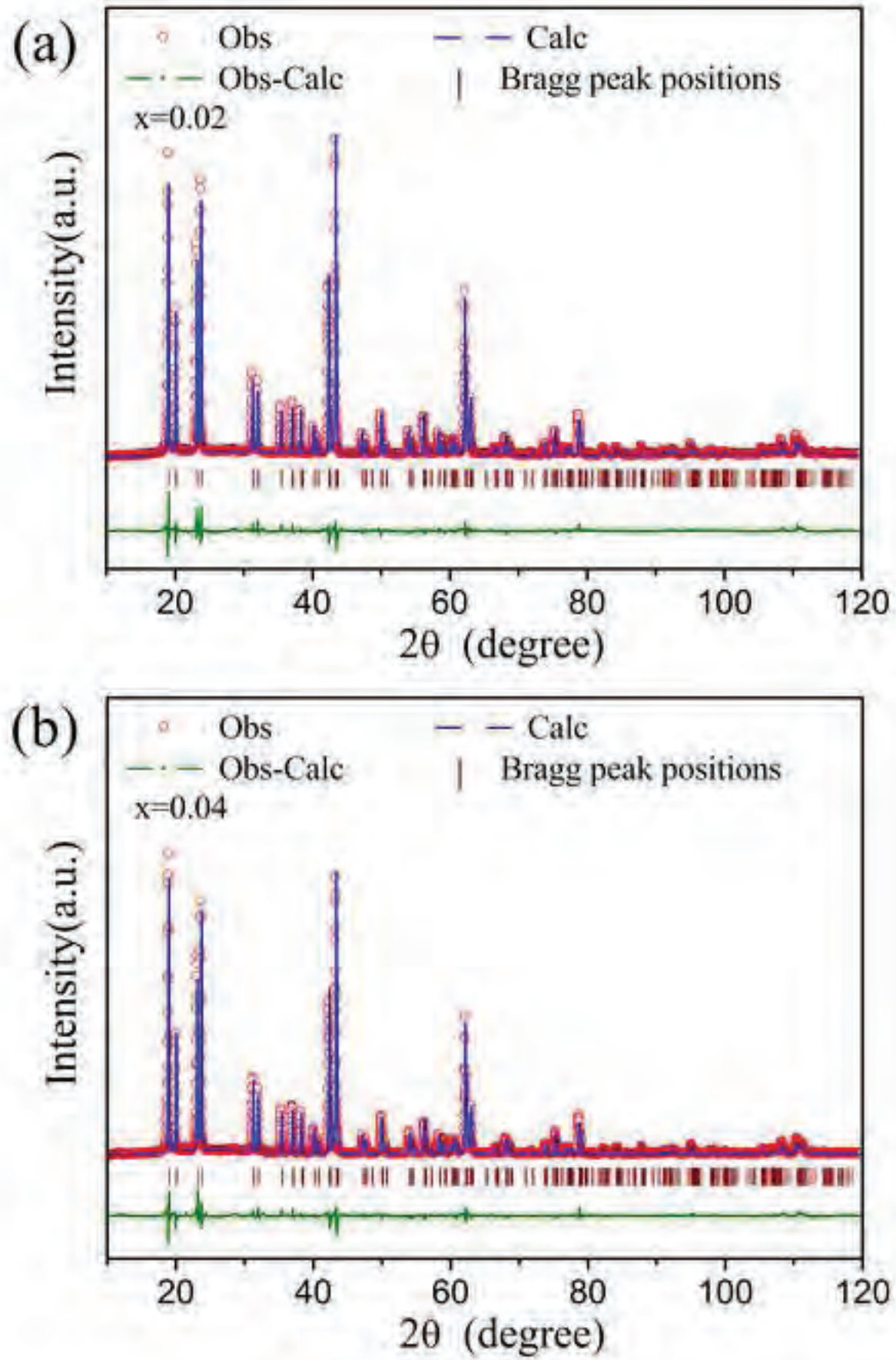

Figure 3

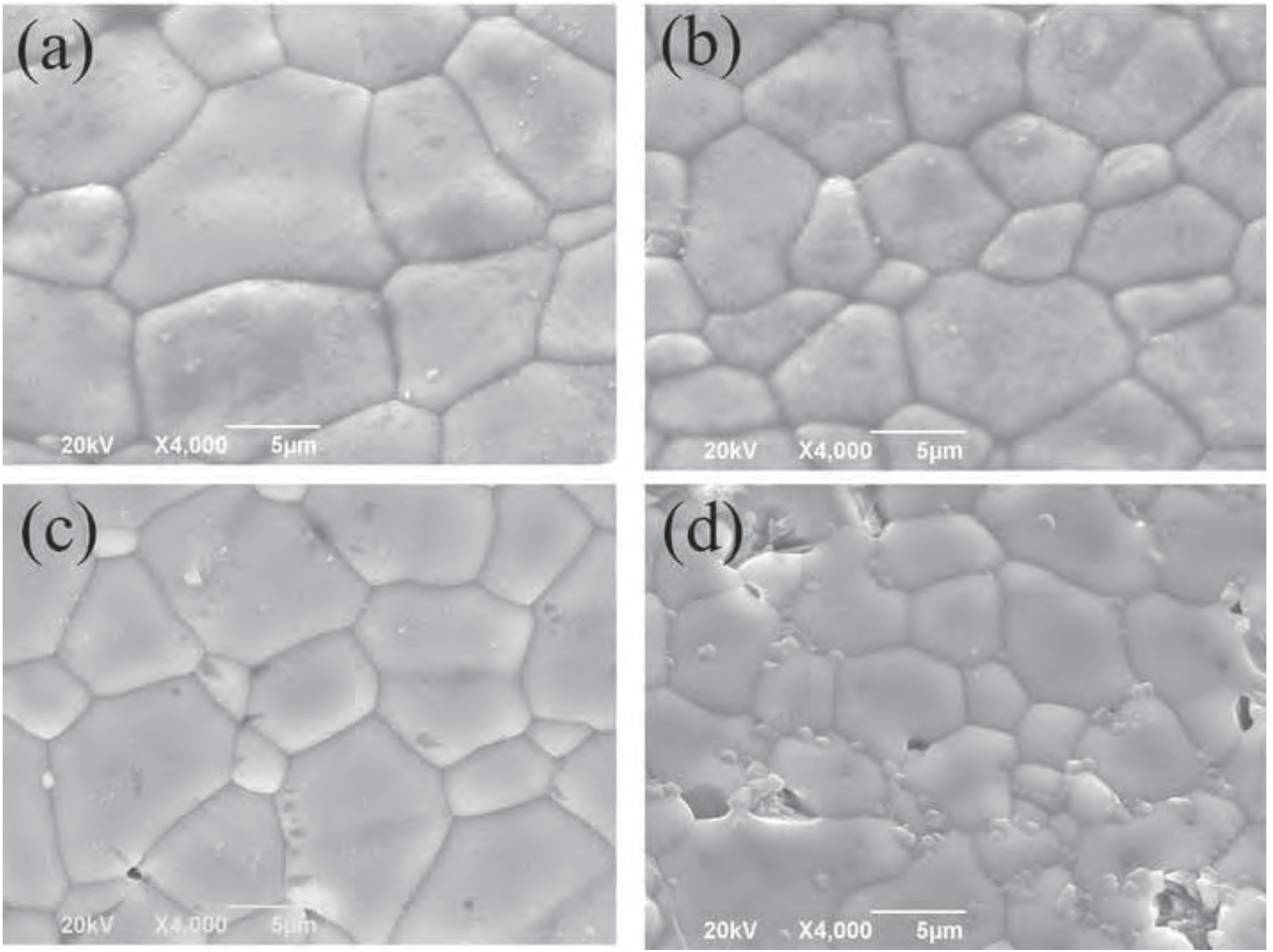

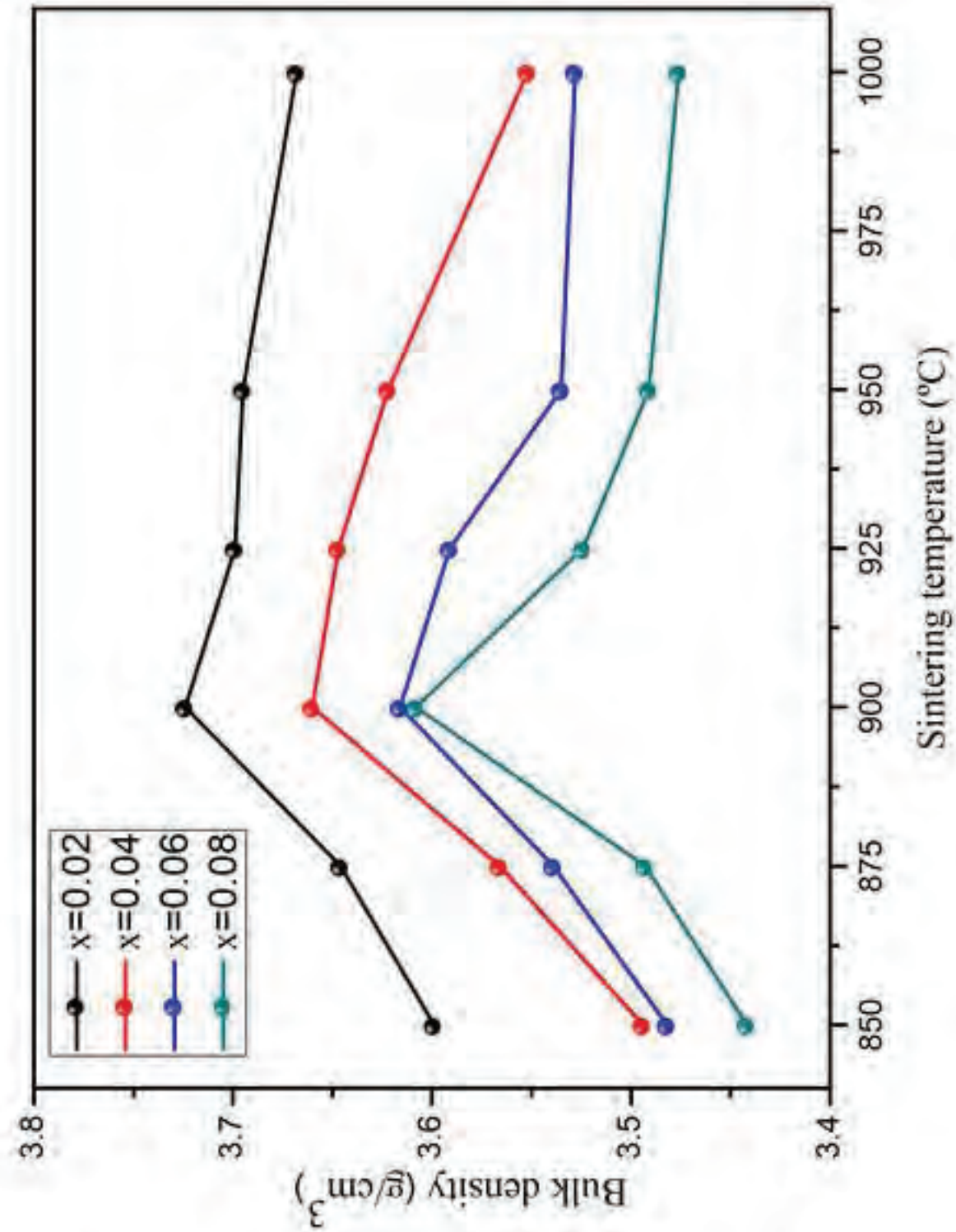
x=0.02
x=0.04
x=0.06
x=0.08
Bulk density (g/cm^3)
Sintering temperature (°C)
3.8
3.7
3.6
3.5
3.4
850
875
900
925
950
975
1000

Figure 4

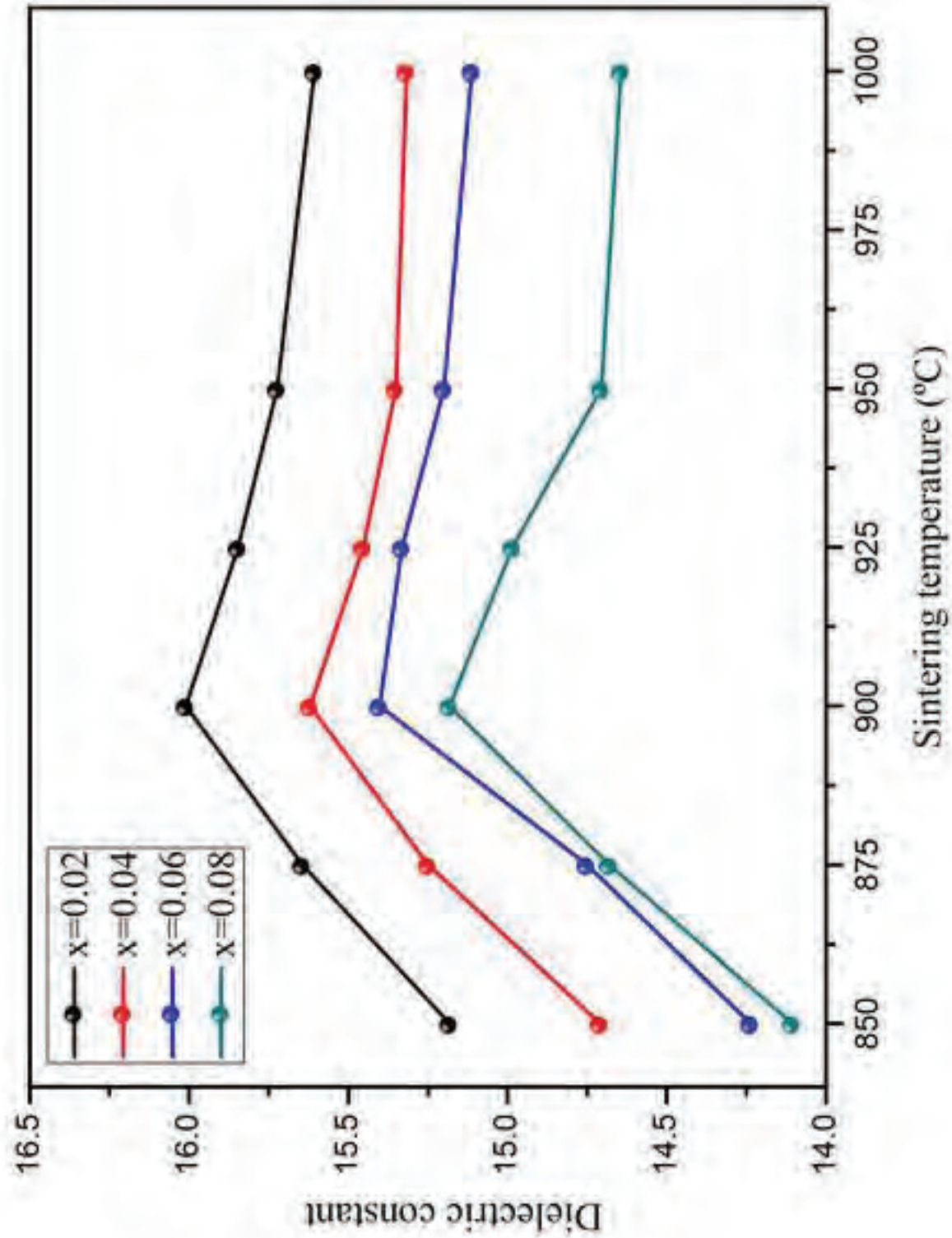
Dielectric constant
Sintering temperature (°C)
x=0.02
x=0.04
x=0.06
x=0.08
16.5
16.0
15.5
15.0
14.5
14.0
850
875
900
925
950
975
1000

Figure 5

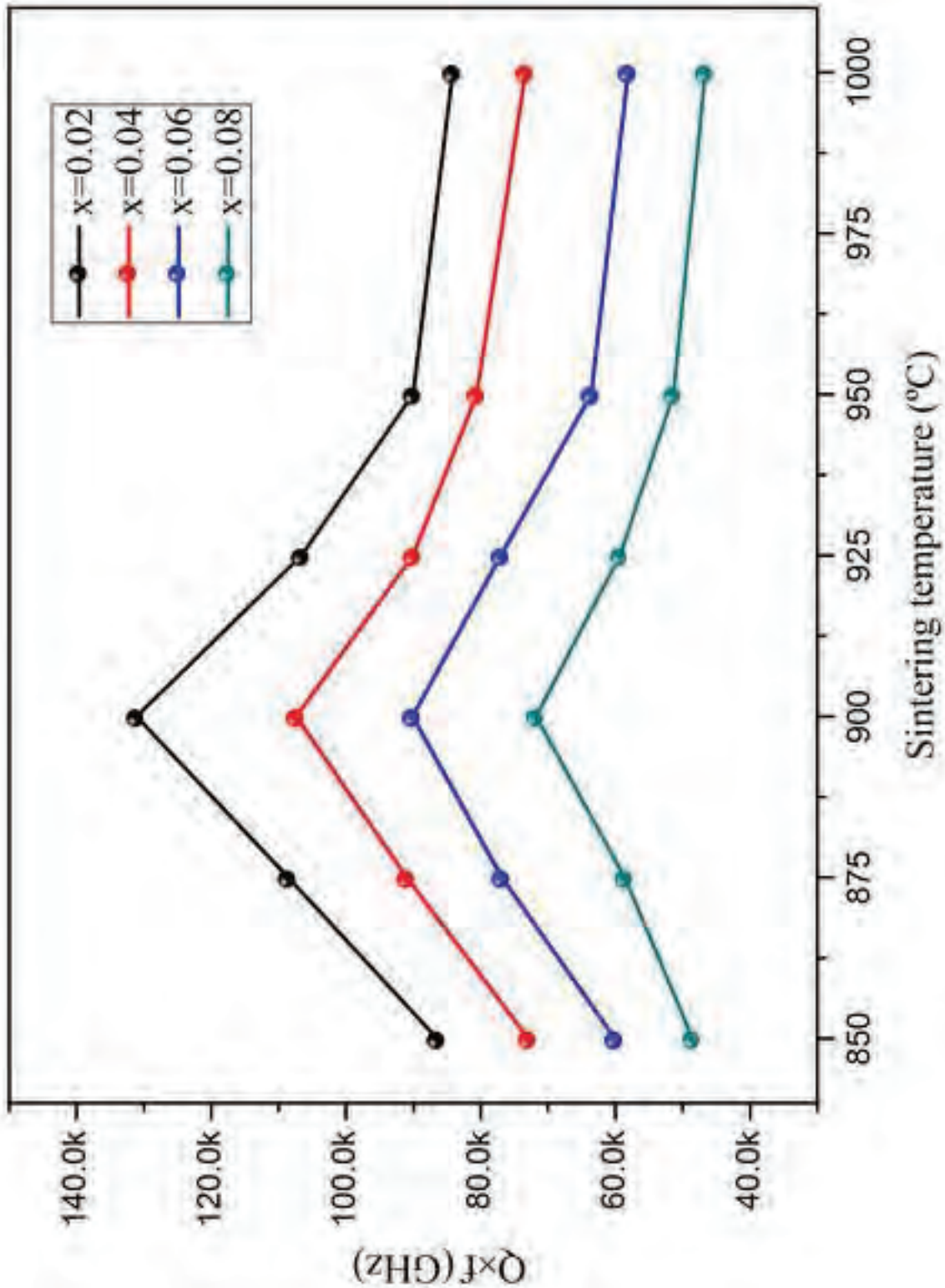
x=0.02
x=0.04
x=0.06
x=0.08
140.0k
120.0k
100.0k
80.0k
60.0k
40.0k
Q×f (GHz)
850
875
900
925
950
975
1000
Sintering temperature (°C)

Figure 6

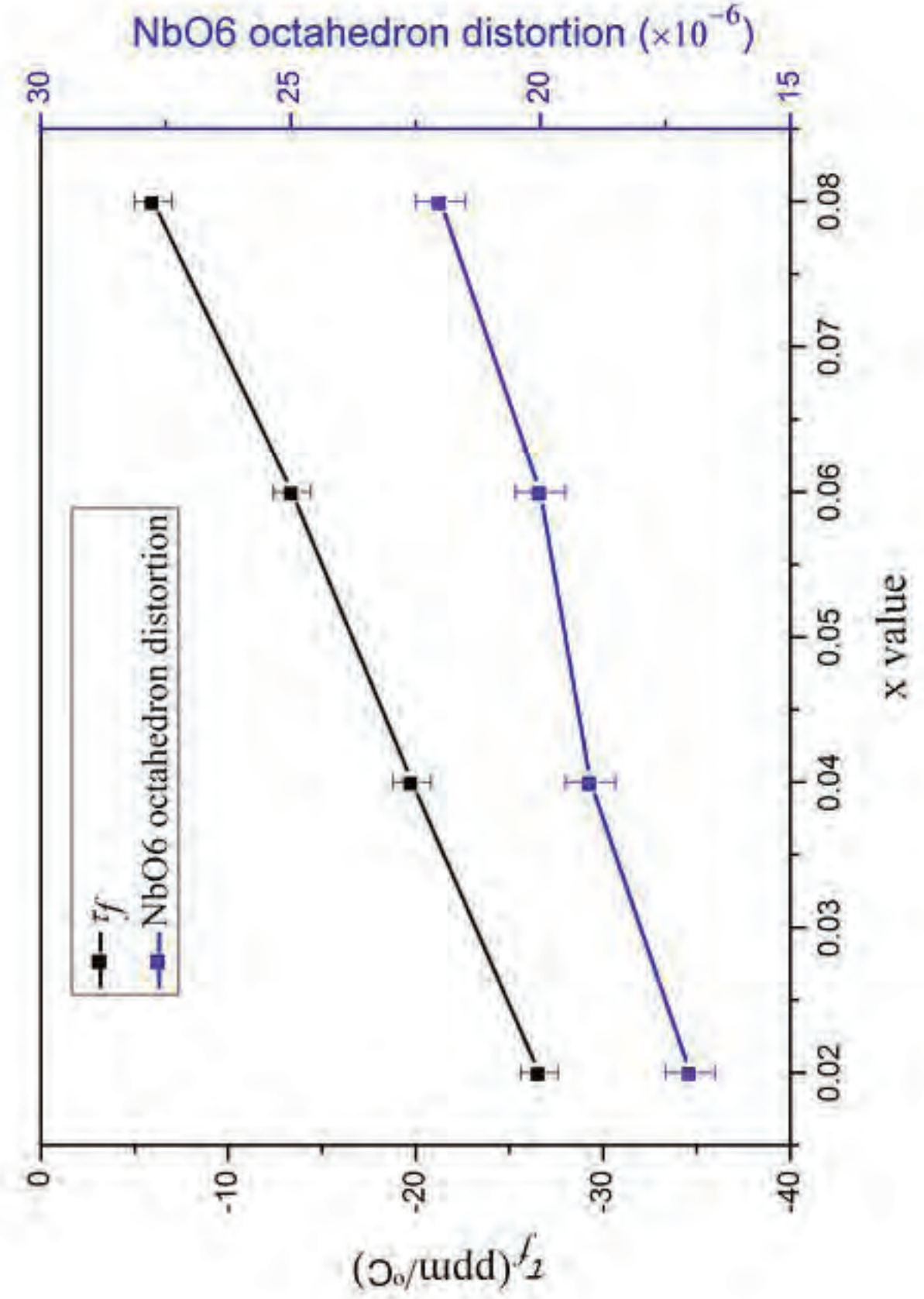
NbO6 octahedron distortion (×10^-6)
30
25
20
15
0
-10
-20
-30
-40
τf (ppm/°C)
0.02
0.03
0.04
0.05
0.06
0.07
0.08
x value
τf
NbO6 octahedron distortion

Figure 7